Mott-enhanced exciton condensation in a Hubbard bilayer

Samuele Giuli [1,*] Adriano Amaricci [2] and Massimo Capone [1,2,†]

[1]*International School for Advanced Studies (SISSA), via Bonomea 265, 34136 Trieste, Italy*
[2]*CNR-IOM Democritos, Istituto Officina dei Materiali, Via Bonomea 265, I-34136 Trieste, Italy*

We study the conditions to realize an excitonic condensed phase in an electron-hole bilayer system with local Hubbard-like interactions at half-filling, where we can address the interplay with Mott localization. Using dynamical mean-field theory, we find that an excitonic state is stable in a sizable region of a phase diagram spanned by the intralayer (U) and interlayer (V) interactions. The latter term is expected to favor the excitonic phase which is indeed found in a slice of the phase diagram with $V > U$. Remarkably, we find that, when U is large enough, the excitonic region extends also for $U > V$, in contrast with naïve expectations. The extended stability of the excitonic phase can be linked to in-layer Mott localization and interlayer spin correlations. Using a mapping to a model with attractive interlayer coupling, we fully characterize the condensate phase in terms of its superconducting counterpart, thereby addressing its coherence and correlation length.

I. INTRODUCTION

The condensation of excitons in a macroscopic quantum state has been proposed soon after the success of the BCS theory of superconductivity [1,2] owing to the similarities between Cooper pairs created by the binding of two electrons and excitons, bound states formed by an electron and a hole. However, the observation of excitonic phases has long eluded the experimental effort, mainly because of the short lifetimes of excitons due to electron-hole recombination processes.

Developments in the engineering of devices and heterostructures have provided ideal platforms to observe exciton condensation (EC), which has been indeed proposed and reported in quantum Hall bilayers [3,4], graphene double bilayers [5–8], and semiconductors quantum wells [9,10]. Excitonic ordering has also been recently reported in bulk solids [11–18].

Bilayer structures are arguably ideal platforms to observe condensation of spatially indirect excitons composed of holes and electrons belonging to different layers, for which recombination is essentially inhibited by the presence of a dielectric material between the layers. Quantum Monte Carlo calculations for electron-hole gases coupled with the long-range Coulomb interaction [19–21] have indeed shown that an excitonic phase is stable at very low densities, a result which has been confirmed by simulations of double bilayer graphene [5,6].

In an analogous lattice model with local interactions, some indication of EC has been found away from half-filling [22] and in the half-filled system when the interlayer interaction is larger than the intralayer repulsion [23,24]. Similar models have been investigated using dynamical mean-field theory (DMFT). In Ref. [25] the competition between EC and *s*-wave superconductivity has been addressed in a model without intralayer repulsion. A variety of two-orbital models including, e.g., energy splitting between bands, Hund's coupling, and including nontrivial topology have also been found to host excitonic states in some regions of parameters [26–31].

In this paper, we aim at identifying a generic mechanism connecting strong correlation physics and excitonic phases which can be used to gain a deeper insight into results on more involved and richer models for specific systems. We address the interplay between the EC and Mott physics, the most direct fingerprint of correlations, in an idealized model for an electron-hole bilayer system with local Hubbard-like interactions. Our focus is on the relative role of the intralayer (U) and interlayer (V) interactions. We consider the system at half-filling, where a Mott transition can take place, so that our phase diagram will be characterized by the competition/interplay between Mott insulating and EC phases. We choose this simplified model, which does not include nonlocal interactions, to disentangle the role of Mott physics in the simplest possible framework. The present results are not meant to describe any specific material, even if this modeling can be considered relevant to transition metal oxides, where the Coulomb interaction is screened, while it is certainly more questionable for semiconductors and graphene bilayers.

The paper is organized as follows: In Sec. II, we introduce the model, our implementation of DMFT, and the relevant observables we consider. In Sec. III, we present the normal phase results where we discard excitonic ordering, while Sec. IV is devoted to the results for the EC phase. Section V reports our concluding remarks.

---
*sgiuli@sissa.it
†capone@sissa.it

II. MODEL AND METHOD

We consider a two-layer Hubbard model with a local interaction term:

$$
\begin{aligned}
H = &- \sum_{\langle ij \rangle \sigma m} t_m c_{i\sigma m}^\dagger c_{j\sigma m} + \text{H.c.} - \mu \sum_{i\sigma m} n_{i\sigma m} \\
&+ U \sum_{im} n'_{i\uparrow m} n'_{i\downarrow m} + V \sum_{i\sigma\sigma'} n'_{i\sigma A} n'_{i\sigma' B},
\end{aligned}
\tag{1}
$$

where $c_{i\sigma m}$ ($c_{i\sigma m}^\dagger$) is the annihilation (creation) operator of an electron on site i, layer $m = A, B$ and with spin σ, $n_{i\sigma m}$ is the number operator, and $n'_{i\sigma m} = n_{i\sigma m} - \frac{1}{2}$ is introduced to write the model in a particle-hole symmetric form which implies that both bands are half-filled for $\mu = 0$. We set $t_A = t$ and $t_B = \alpha t_A$. In our calculations, we will consider $\alpha = -1$, so that the A band has a standard negative hopping amplitude, and it is an electronlike character around $q = 0$, while the B band has a positive hopping amplitude, and it has a holelike character around $q = 0$. We notice in passing that, for a bipartite lattice (with sublattices S_1 and S_2), a sign-change transformation on one of the sublattices for the B band:

$$
c_{iB}^\dagger, c_{iB} \rightarrow -c_{iB}^\dagger, -c_{iB} \ \forall i \in S_1,
\tag{2}
$$

would change the sign of the hopping, leading to two identical bands. Here, U and V are both positive, and they measure the intralayer and interlayer local screened Coulomb repulsion.

We will study an excitonic state characterized by a uniform ($q = 0$) spin-singlet excitonic order parameter (EOP):

$$
\Delta_0 = \frac{1}{N} \sum_{i\sigma} \langle c_{iA\sigma}^\dagger c_{iB\sigma} \rangle,
\tag{3}
$$

which is expected to be degenerate with spin-triplet counterparts due to the $SU(2) \times SU(2)$ spin symmetry of our model. Models including other interaction terms and material-specific features may favor one or the other spin symmetry [28,29,31]. On the other hand, we will not consider the possibility of staggered spin, charge, or orbital orderings. A staggered orbital ordered state can compete with the EC, and it is expected to be stable on bipartite lattices when $V > U$. The choice to discard these orderings is meant to focus on the intrinsic correlation effects which occur regardless of the nature of the lattice, following a standard strategy in the field.

We solve the model at zero temperature using DMFT [32], a state-of-the-art method which treats different interactions nonperturbatively, and it is particularly well suited to study the Mott transition [32], strongly correlated metallic phases, as well as superconductivity and other broken-symmetry states. Within DMFT, the lattice model is mapped onto an impurity model which must be solved self-consistently, requiring that the impurity Green's function coincides with the local component of the lattice Green's function. We solve the impurity model at $T = 0$ using Lanczos/Arnoldi exact diagonalization (ED) [33–35]. As is customary in the DMFT community, we consider a Bethe lattice with a semicircular density of states $N_m(\epsilon) = \frac{2}{\pi D_m^2} \sqrt{D_m^2 - \epsilon^2}$, where $D_m \propto t_m$ is the half-bandwidth.

To study the EC phase, the bath of the impurity model must include an excitonic amplitude, analogous to the superconducting case. Using a spinorial representation where $\Psi_{k,\sigma}^\dagger = (c_{k\sigma A}^\dagger, c_{k\sigma B}^\dagger)$, where $k = 0$ identify the impurity and $k = 1, ..., N_{\text{bath}}$ the bath levels, we can write it as

$$
H_{\text{imp}}^{(0)} = \sum_{k\sigma} \begin{pmatrix} \Psi_{k\sigma}^\dagger & \Psi_{0\sigma}^\dagger \end{pmatrix} \begin{pmatrix} \mathcal{H}_{k\sigma} & V_k \cdot \mathbb{I}_2 \\ V_k \cdot \mathbb{I}_2 & 0 \end{pmatrix} \begin{pmatrix} \Psi_{k\sigma} \\ \Psi_{0\sigma} \end{pmatrix}, \tag{4}
$$

where $\mathbb{I}_2$ is the 2×2 identity, and

$$
\mathcal{H}_{k\sigma} = \begin{pmatrix} \epsilon_k + M_k & P_k \\ P_k & \epsilon_k - M_k \end{pmatrix},
\tag{5}
$$

where P_k is the interorbital excitonic hybridization term in the bath Hamiltonian, $\epsilon_k + (-)M_k$ is the bath energy on orbital A (B), and V_k is the hybridization between the impurity and bath site k. Within ED-DMFT, we must limit the number of bath sites to solve the impurity model. We fixed the number of bath sites to $N_{\text{bath}} = 4$, and we have checked that the numerical error introduced by the finite bath is sufficiently small. We fixed the system at global half-filling $\langle \sum_{\sigma m} n_{\sigma m} \rangle = 2$ by imposing $\mu = 0$. Then since we are focusing on orbitals with opposite dispersion relation, we also fixed $\epsilon_k = 0 \ \forall k$, and since we focus on the state with orbital half-filling, this required that, for each M_k parameter on bath site k, there must be another bath site k' with opposite energy $M_{k'} = -M_k$.

III. NORMAL STATE

We start our investigation from the normal state where we inhibit excitonic ordering as well as any other broken-symmetry state like antiferromagnetism or staggered orbital ordering. This is a standard strategy which has helped us to understand the Mott transition disentangling Mott localization from magnetic ordering [32]. For our model, a normal state phase diagram has been reported in Ref. [36], but we find it useful to present our results to emphasize the aspects which are useful to better address the excitonic phase.

The model is expected to feature two different Mott-insulating solutions that we can easily understand from the atomic ($t_m = 0$) limit. Among all configurations with two electrons per site, the four with one electron in each layer $|\uparrow, \downarrow\rangle$, $|\downarrow, \uparrow\rangle$, $|\uparrow, \uparrow\rangle$, and $|\downarrow, \downarrow\rangle$ have energy $E_{11} = -\frac{1}{2}U$, while the two configurations with two electrons in the same layer $|\uparrow\downarrow, 0\rangle$ and $|0, \uparrow\downarrow\rangle$ have energy $E_{20} = \frac{1}{2}U - V$. Therefore, the former set of states is favored for $U > V$ and the latter for $U < V$. Hence, when U and V are much larger than the hopping and $U > V$, we expect an insulator with one electron on every site of each layer. This state, that we label as U-Mott (U-MI) is expected to be unstable toward antiferromagnetic ordering if we allow for symmetry breaking. On the other hand, for $V > U$, we have an insulator where every site is in a mixture between the two solutions with one doubly occupied layer. This state, henceforth V-Mott (V-MI), would be naturally unstable toward a staggered orbital (layer) ordering [37].

To monitor the Mott localization, we compute the quasiparticle weight Z_m which measures the metallicity of the system [32]. The progressive destruction of the metallic state is described by a reduction of Z_m from 1 (noninteracting limit) to 0 (correlated insulator). The connected local density-density correlations $C_{m,m'} = \langle n_m n_{m'} \rangle - \langle n_m \rangle \langle n_{m'} \rangle$ can be used to study the competition between the two interaction terms and the
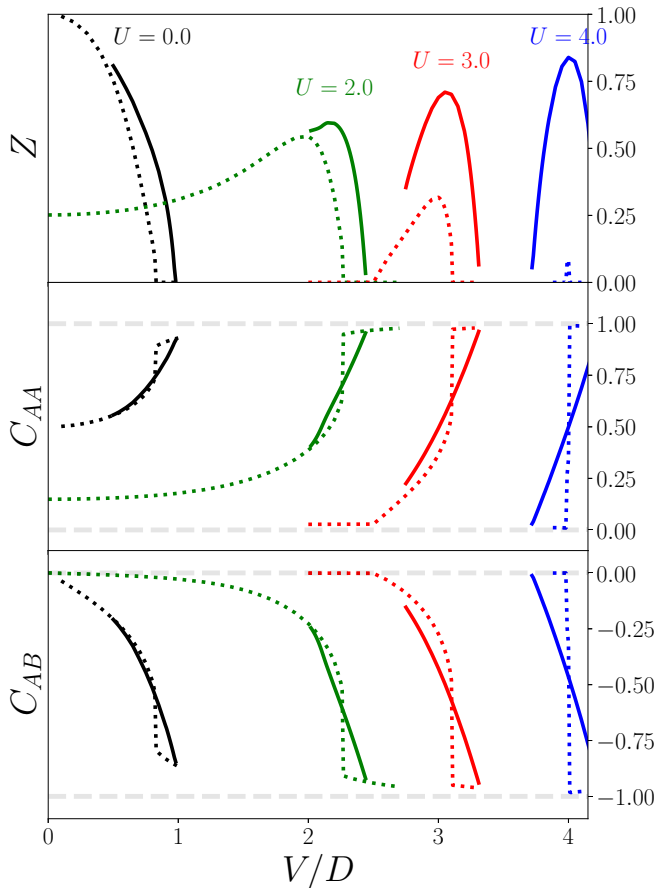
FIG. 1. Quasiparticle weight (top), intraorbital density-density correlation (center) and interorbital density-density correlation (bottom), as a function of V/D for $U/D = 0.0$ (black), 2.0 (green), 3.0 (red), and 4.0 (blue). Dotted lines are data in the normal state, solid lines mark the same quantities in the excitonic phase. The gray dashed lines are the atomic limits.

FIG. 2. V vs U ground state phase diagram. In yellow, the region of the exciton condensation (EC) phase; in orange, the metallic phase; in blue, the U-Mott insulator; and in green, the V-Mott one. The dashed lines with crosses symbols indicate the two Mott-transition boundaries in the normal state, while the gray dashed line highlights the $U = V$ line.

competition between different atomic states leads to intermediate phases which can have either a metallic [39,40] or an insulating [41] nature.

IV. EXCITONIC PHASE

We now turn to solutions where the EC is allowed. The values of Z_A, C_{AA}, and C_{AB} are shown as solid lines in Fig. 1 and compared with their normal state counterparts. Indeed, the excitonic state is stable in a wide region of parameters, and its onset makes the evolution from U-MI to V-MI smoother, thereby also increasing the quasiparticle weight.

Reporting this information on the phase diagram of Fig. 2, where the boundaries of the excitonic region are solid black lines, we clearly see that the EC region is roughly centered around the normal state transition toward the V-Mott state. The picture is simple: Increasing V before the interaction is large enough to drive the system to insulating leads to the binding of electrons and holes on different layers into excitons. However, the effect of U changes the position and the nature of the transition.

For small and moderate U, the EC establishes only when V prevails over U (above the $V = U$ line, marked with a dashed gray line) in agreement with previous work [23–25]. We notice that we find an unambiguous excitonic solution for $U = 0$ only when V is larger than a critical value. Indeed, we cannot rule out the possibility of an exponentially small order parameter that we cannot easily resolve with our algorithm which has an intrinsic low-energy cutoff.

A much less expected result emerges when we increase U and approach the boundary of the U-MI phase. Here, we find

approach to the atomic limit insulators. The orbital symmetry implies $C_{AA} = C_{BB}$ and $C_{AB} = C_{BA}$. It is easy to see from the above discussion that the atomic U-MI has $C_{AA} = 0$ and $C_{AB} = 0$, while the atomic V-MI has $C_{AA} = 1$ and $C_{AB} = -1$.

In Fig. 1, we show as dotted lines the evolution of $Z_A = Z_B$ and of the interlayer and intralayer correlations C_{AA} and C_{AB} as functions of V/D for different values of U/D. The boundaries of the U-MI and V-MI phases are marked by dotted lines with crosses in the phase diagram of Fig. 2.

The cuts for $U/D = 0$ and 2 in Fig. 1 clearly show a metal-insulator transition toward the V-MI state with $Z_A = 0$, $C_{AA} = 1$, and $C_{AB} = -1$. For $U/D = 3$, we find a U-MI for small V followed by a metallic region and the V-MI as V increases. For large $U/D = 4$, we have only a tiny slice of V with a metallic solution sandwiched by the two insulators.

The main feature of the normal state phase diagram, as already pointed out in Ref. [36], is the existence of a metallic region that intrudes between the two insulators when U and V are comparable. The region shrinks as we increase U and V, and it closes for $U = V = 4$, where we find a tricritical point. For larger values of the interactions, the metallic solution is confined to the line $U = V$, like other models where the
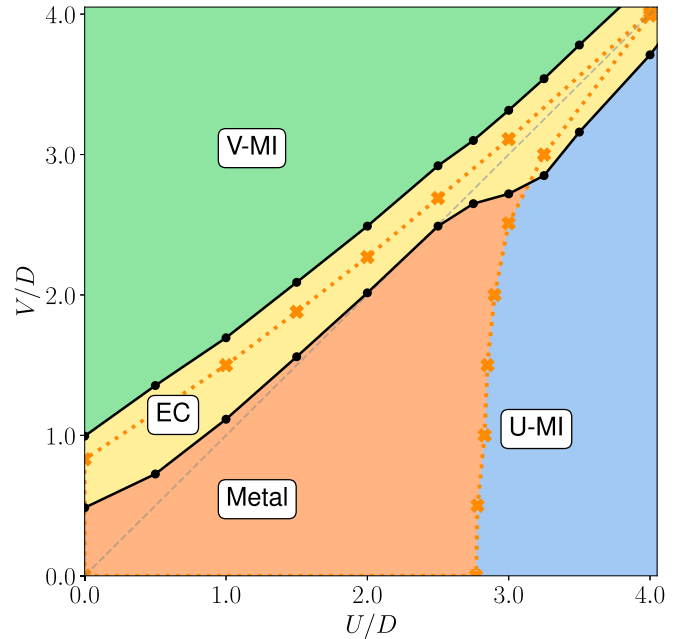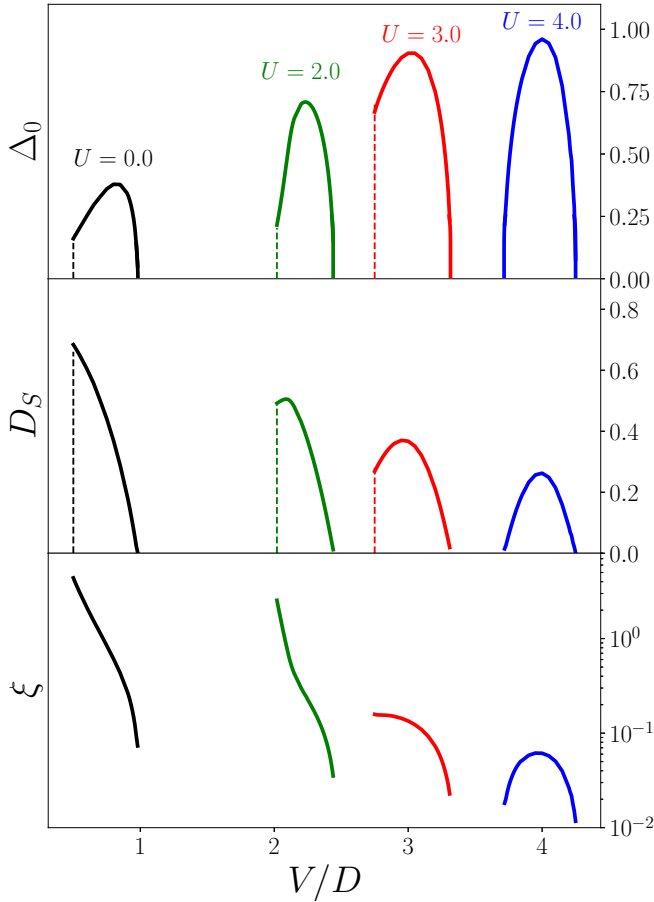
FIG. 3. Excitonic order parameter Δ_0 (top), stiffness D_s (center), and coherence length ξ for (from left to right) $U/D = 0.0, 2.0, 3.0,$ and 4.0, with the same color codes as Fig. 1. The vertical dashed line indicates the first-order metal-exciton condensation (EC) phase transition.
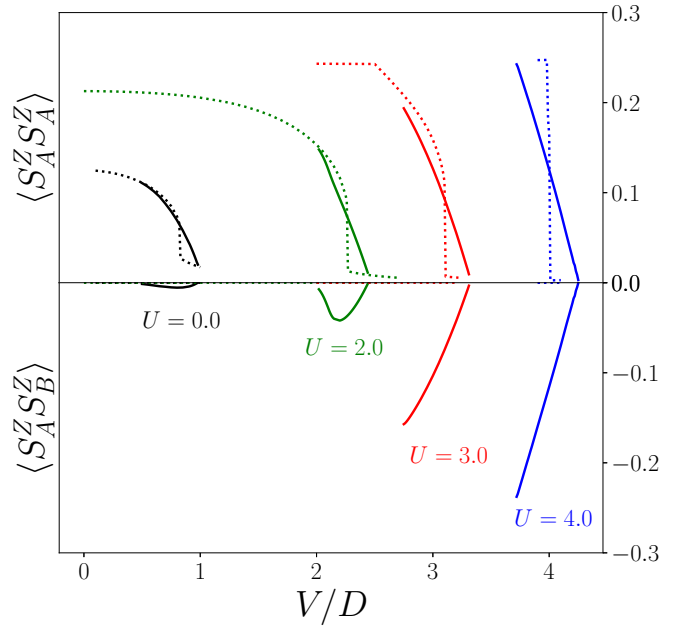

FIG. 4. Local magnetic moments (intraorbital spin correlations) (top) and interorbital magnetic correlation (bottom). Dotted and solid lines indicate, respectively, the normal and the excitonic phase solution. Data are for $U/D = 0.0$ (black), 2.0 (green), 3.0 (red), and 4.0 (blue).

that the stability region of the EC increases, and remarkably, it extends into the region where $U < V$, signaling a nontrivial intrinsic many-body effect due to the interplay of the two interactions. As a result, for $U \gtrsim 3D$, the whole metallic region between the two Mott insulators is replaced by an excitonic state.

The positive effect of Hubbard repulsion on the excitonic order is evident in Fig. 3(a), where we plot the order parameter Δ as a function of V for the same cuts of Fig. 1. Here, we show that the EC for large U is not only stable in a wider range of V, but its amplitude is also larger. For instance, for $U/D = 4$, the maximum value of Δ is more than twice the $U = 0$ maximum. For every value of U, the transition from the metal to the EC appears of first order, while the transition from the EC to the V-MI state is associated with a continuously vanishing Δ.

A. Exciton ordering and Mott physics

In this section, we link the enhancement of the EC region for $V < U$ and large U/D to the magnetic correlation between orbitals near the V-MI phase that is enhanced by the nearby U-MI phase. The main effect of U is to drive a standard Mott localization within each layer. Hence, the

double occupation on each layer d_m is strongly reduced. For a half-filled nonmagnetic system, this directly reflects in the formation of local moments as measured by $\langle S_m^z S_m^z \rangle = \frac{1}{4}\langle (n_{m,\uparrow} - n_{m,\downarrow})^2 \rangle = \frac{1}{2}(\frac{1}{2} - d_m)$, which approaches $\frac{1}{4}$. While the spins on the two layers are uncorrelated in the normal state, when we reach the EC region and $U \gtrsim 3D$, the interlayer spin correlations $\langle S_A^z S_B^z \rangle$ become sizable and negative, eventually approaching the limit $-\frac{1}{4}$, as shown in Fig. 4. The local quantum state (computed from the impurity model within DMFT) approaches for large $U |\psi\rangle \sim \frac{1}{\sqrt{2}}(|\uparrow_A \downarrow_B\rangle + |\uparrow_B \downarrow_A\rangle)$, for which $\langle S_A^z S_A^z \rangle = \frac{1}{4}$ and $\langle S_A^z S_B^z \rangle = -\frac{1}{4}$.

Note, however, that the interplay between Mott localization and exciton ordering is not trivial. The singlet atomic excitonic state is indeed a linear combination of $|\uparrow_A \downarrow_B\rangle$ and $|\uparrow_B \downarrow_A\rangle$, which are favored by increasing U, but also of the states $|\uparrow_A \downarrow_A, 0\rangle$ and $|0, \uparrow_B \downarrow_B\rangle$, which are instead depleted by U. Hence, while the magnetic correlations develop approaching the U-Mott state, they first contribute to the onset of excitonic ordering, but as we exceed a given optimal distance from the Mott state, the EOP decreases, leading to the existence of a bell-shaped behavior of the order parameter.

We finally notice that the spin-singlet correlations follow from our choice to study spin-singlet excitons, and we expect the same picture to hold for a spin-triplet exciton. The key idea is that Mott localization within each layer leads to localized moments which are naturally prone to acquire any interlayer correlation when exciton ordering is allowed. Finally, in the U-MI state, the EOP vanishes, and the SU(2) $\times$ SU(2) spin symmetry with four independent ground states is recovered.

B. Characterizing the excitonic state via a mapping on superconductivity

A particle-hole transformation on layer B:

$$c_{i\sigma B}^{\dagger} \rightarrow c_{i\sigma B}(-1)^{\sigma}, \tag{6}$$

maps our model for $\alpha = -1$ onto a two-orbital model with the same form of Eq. (1), in which the two orbitals share the same hopping $t_A = t_B = t$, and the interorbital interaction becomes attractive $(-V)$, while the intralayer remains repulsive. This model can indeed host an interorbital s-wave superconducting state, which maps onto our excitonic state via the same particle-hole transformation in Eq. (6). We can exploit this mapping to compute some observable which characterizes the superconducting state and allows us to better characterize the EC.

The superfluid stiffness D_s [42] is a crucial parameter that controls the critical temperature. It measures the coherence of the superconducting state and its rigidity to fluctuations of the phase of the order parameter. Indeed, a superconductor with small D_s has a small critical temperature, even if the zero-temperature absolute value of the order parameter is large, as it happens in the strong-coupling limit in a single-orbital attractive Hubbard model [43]. In the effective model with interlayer attraction $-|V|$ obtained via the transformation in Eq. (6), D_s reads

$$\frac{D_S}{\pi e^2} = \langle -E_{\text{kin}} \rangle - \chi_{jj}(\mathbf{q} \rightarrow 0, \omega = 0), \tag{7}$$

where j is the current operator and E_{kin} is the expectation value of the hopping part of the Hamiltonian. For a Bethe lattice, we obtain [43]

$$\frac{D_S^{\text{ex}}}{e^2\pi} = -\frac{4\alpha}{\beta} \sum_{i\omega_n,\sigma} \int d\varepsilon V(\varepsilon) D(\varepsilon) |G_{AB}(\varepsilon, i\omega_n)|^2, \tag{8}$$

where $V(\epsilon) = \frac{4t^2 - \epsilon^2}{2}$ is the square of the current vertex for orbital A and $\alpha = t_B/t_A$ (see Appendix A for derivation).

We underline that the total current of the attractive model corresponds, in the model in Eq. (1), to the operator:

$$j_{\text{ex}}(\mathbf{q}, i\omega_n) = j_A(\mathbf{q}, i\omega_n) - j_B(\mathbf{q}, i\omega_n), \tag{9}$$

which is clearly different from the current operator associated with the total charge. Hence, D_s can be considered a real superfluid stiffness only for the auxiliary attractive model.

However, D_s also provides direct information about the coherence and stability properties, which translates into analogous information about the EC phase of our model in Eq. (1). It has been shown that quantum geometry could play a role in enhancing the superfluid stiffness [44], but we only consider the full contribution.

The coherence length ξ indeed naturally has the same meaning in the two frameworks, namely, it measures the length over which the constituents of the pair/exciton retain quantum coherence. It is given by [45,46]

$$\xi^2 = \frac{\sum_{\mathbf{k}} |\nabla_{\mathbf{k}} F(\mathbf{k})|^2}{\sum_{\mathbf{k}} |F(\mathbf{k})|^2}, \tag{10}$$

where

$$F(\mathbf{k}) = \sum_{i\omega_n} \exp(i\omega_n 0^+) G_{AB}(\epsilon_{\mathbf{k}}, i\omega_n). \tag{11}$$

The results for D_s and ξ are reported in panels (b) and (c) of Fig. 3 to compare their behavior with the EOP. The results for $U = 0$ are qualitatively like an attractive model, and they reflect the BCS-to-Bose-Einstein condensate (BEC) crossover as a function of the coupling. Indeed, both D_s and ξ are maximal in the weak-coupling side, and they decrease as the interaction grows.

Increasing $|V|$, we have a progressive reduction of the coherence length, associated with a more localized pairs/excitons characteristic of the BEC limit. Also, D_s decreases as a result of the smaller coherence of the pairs/excitons, and it vanishes at the continuous transition to the V-MI state.

When we introduce and increase U, we find an important difference on the weak-coupling side of the crossover. Indeed, both D_s and ξ are also depleted close to the smallest values of V required to establish the EC. As a result, for large U, the two quantities have a maximum around the $U \sim V$ line. These results clearly confirm the U-induced localization of the excitons that we discussed above and the crucial role of the interplay between the two interactions to induce an EC for $V < U$.

V. CONCLUSIONS

We used DMFT to assess the existence of an excitonic state in the zero-temperature phase diagram of a two-layer Hubbard model with intralayer (U) and interlayer (V) density-density repulsive interactions. Working at half-filling, we can study how the excitonic long-range order is affected by the Mott physics.

We find a sizable region of exciton ordering when the two interactions are comparable. The transition from the EC phase to the Mott insulating phase is continuous, while the transition from metal to EC is of the first order.

For small and intermediate U, the excitonic state is present only if $V > U$, as one can expect intuitively. On the other hand, for $U \gtrsim 3D$, i.e., close to a standard Mott transition within each layer, we also find an exciton state when $V < U$. We have indeed shown that the enlargement of the excitonic phase in the proximity of the intralayer Mott transition can be connected with the U-driven development of local magnetic moments that, in turn, favor magnetic correlations between the two layers (singlets in our case). We expect this mechanism to be general and to also be present for models where the exciton and the magnetic correlations have a triplet symmetry.

This interaction-driven stabilization of the excitonic state is clearly associated with the proximity to the Mott transition, and it is accompanied by the development of spin correlations between the layers. These effects cannot be described by a static mean-field calculation, which indeed does not show the extension of the excitonic region. In this sense, the stabilization of excitons for $V < U$ is due to dynamical quantum correlations which are included in DMFT via frequency-dependent self-energies. Notice that these dynamical effects are nonperturbative, as DMFT contains corrections at any order within a momentum-independent self-energy.

Exploiting a simple mapping onto a model with attractive interlayer interactions, we have been able to further characterize the excitonic state. The coherence length, which

has essentially the same interpretation of that of a supercon-ductor, shows that the proximity to the V-driven Mott state leads to localized pairs with very short coherence length. Analogously, the equivalent of the superconducting superfluid stiffness shows that the coherence of the EC state tends to vanish when the V-Mott insulator is reached. In other words, when we approach the Mott transition, the EC state is driven toward the strong-coupling limit, which in superconducting language corresponds to the BEC limit [43]. We notice in passing that the BEC nature and its evolution from a BCS limit can be experimentally assessed via both thermodynamic [43] and spectral properties [47,48]. These results further strengthen our picture where the charge localization induced by U is central in the stabilization of the EC for $V < U$ and in determining its properties.

The existence of excitonic states for $V < U$ is important because, in a real bilayer system or in a multiorbital correlated material, we always expect $V < U$. We notice, however, that an electron-phonon coupling of the Holstein type (coupled with the total local electron density) can effectively reduce U, making in principle the effective U closer or even smaller than V [41,49,50].

We emphasize that we have decided not to consider spatially ordered states to highlight the general mechanism connecting Mott physics with EC which are realized in a generic lattice. In a bipartite lattice, a staggered orbital order is stable for $V > U$, partially covering the excitonic region. However, the most important region where the EC is favored by the proximity to the Mott transition is not affected.

As we anticipated in the introduction, our model has been introduced as a minimal model for a bilayer system in which excitonic phases can be present and, at the same time, Mott physics is effective. The results we have obtained must be considered as a basis to build the understanding of richer and more involved models including, among others, different and more complex hopping structures, energy difference, and/or hybridization between the two bands and a richer structure of the interactions. Even if our results are directly relevant for any specific material because of the simplicity of the model, they can provide a solid basis for the research of materials where the Coulomb interaction is strongly screened, such as transition metal oxides or twisted transition metal dichalco-genides where narrow moiré bands can be obtained.

APPENDIX A: SUPERFLUID STIFFNESS

In this Appendix, we provide some details for the cal-culation of the superfluid stiffness for the attractive model obtained through the canonical transformation in Eq. (6). From the definition [42]:

$$\frac{D_S}{\pi e^2} = \langle -E_{\text{kin}} \rangle - \chi_{jj}(\mathbf{q} \to 0, \omega = 0). \qquad (A1)$$

we need to compute the kinetic energy and the current-current response function. We make use of the previously defined spinorial representation to define the Green's function as

$$\hat{G}_\sigma(\mathbf{k}, \tau) = \left\langle T \begin{bmatrix} c_{kA\sigma}(\tau) \\ c_{kB\sigma}(\tau) \end{bmatrix} \otimes \begin{bmatrix} c_{kA\sigma}^\dagger(0) & c_{kB\sigma}^\dagger(0) \end{bmatrix} \right\rangle = \begin{bmatrix} G_{AA}(\mathbf{k}, \tau) & G_{AB}(\mathbf{k}, \tau) \\ G_{BA}(\mathbf{k}, \tau) & G_{BB}(\mathbf{k}, \tau) \end{bmatrix}. \qquad (A2)$$

From now on, we consider it diagonal in the spin; therefore, we can avoid explicitly writing the spin index σ. In single-site DMFT, where the self-energy is local and site independent, the Dyson equation for the interacting Green's functions reads

$$\hat{G}_0(\mathbf{k}, i\omega_n)^{-1} = \hat{G}(\mathbf{k}, i\omega_n)^{-1} + \hat{\Sigma}(i\omega_n), \qquad (A3)$$

where the hat indicates that all of these are matrices as in the previous Eq. (A2). This means that the diagonal and of-diagonal component are

$$G_{AA}(\varepsilon, i\omega) = \frac{i\omega - \alpha\varepsilon - \Sigma_{BB}(i\omega)}{[i\omega - \varepsilon - \Sigma_{AA}(i\omega)][i\omega - \alpha\varepsilon - \Sigma_{BB}(i\omega)] - |\Sigma_{AB}(i\omega)|^2}, \qquad (A4)$$

$$G_{BB}(\varepsilon, i\omega) = \frac{i\omega - \varepsilon - \Sigma_{AA}(i\omega)}{[i\omega - \varepsilon - \Sigma_{AA}(i\omega)][i\omega - \alpha\varepsilon - \Sigma_{BB}(i\omega)] - |\Sigma_{AB}(i\omega)|^2}, \qquad (A5)$$

$$G_{AB}(\varepsilon, i\omega) = \frac{\Sigma_{AB}(i\omega)}{[i\omega - \varepsilon - \Sigma_{AA}(i\omega)][i\omega - \alpha\varepsilon - \Sigma_{BB}(i\omega)] - |\Sigma_{AB}(i\omega)|^2} = G_{BA}^*(\varepsilon, i\omega), \qquad (A6)$$

where $\alpha = t_B/t_A$; therefore, $\epsilon^{(A)} = \epsilon$ and $\epsilon^{(B)} = \alpha\epsilon$.

In this derivation, we will set the energy splitting to zero ($M = 0$) for simplicity, but the results remain valid for any value of M. In DMFT, the kinetic energy for orbital m can be easily computed since the Green's function is known:

$$
\begin{aligned}
E_{kin}^{(m)} &= \sum_{\mathbf{k}\sigma} \epsilon_{\mathbf{k}}^{(m)} \langle c_{\mathbf{k}\sigma m}^{\dagger} c_{\mathbf{k}\sigma m} \rangle \\
&= \lim_{\eta \to 0^+} \beta^{-1} \sum_{i\omega_n} \sum_{\mathbf{k}\sigma} \epsilon_{\mathbf{k}}^{(m)} G_{mm}(\mathbf{k}, i\omega_n) \exp(i\omega_n \eta) \\
&= \lim_{\eta \to 0^+} \beta^{-1} \sum_{i\omega_n, \sigma} \int d\epsilon D(\epsilon) \epsilon^{(m)} G_{mm}(\epsilon, i\omega_n) \exp(i\omega_n \eta),
\end{aligned}
\tag{A7}
$$

computing it explicitly for the two orbitals and performing a partial integration using the relation $-\epsilon D(\epsilon) = \partial_\epsilon [D(\epsilon) V(\epsilon)]$, where $V(\epsilon) = \frac{4t^2 - \epsilon^2}{3} = [v_\epsilon^{(A)}]^2$ is the square of the current vertex in orbital A, $\alpha^2 V(\epsilon) = [v_\epsilon^{(B)}]^2$ is the square of the current vertex in orbital B, and $D(\epsilon) = \frac{1}{2\pi t^2}\sqrt{(2t)^2 - \epsilon^2}$ is the density of states:

$$
\begin{aligned}
E_{\text{kin},A} &= \beta^{-1} \sum_{i\omega_n, \sigma} \int d\varepsilon\, V(\varepsilon) D(\varepsilon) G_{AA}^2(\varepsilon, i\omega_n) \left\{ 1 + \alpha \frac{|\Sigma_{AB}(i\omega_n)|^2}{[i\omega_n - \alpha\varepsilon - \Sigma_{BB}(i\omega_n)]^2} \right\} \\
&= \beta^{-1} \sum_{i\omega_n, \sigma} \int d\varepsilon\, V(\varepsilon) D(\varepsilon) \left[G_{AA}^2(\varepsilon, i\omega_n) + \alpha |G_{AB}(\varepsilon, i\omega_n)|^2 \right],
\end{aligned}
\tag{A8}
$$

$$
\begin{aligned}
E_{\text{kin},B} &= \beta^{-1} \sum_{i\omega_n, \sigma} \int d\varepsilon\, V(\varepsilon) D(\varepsilon) G_{BB}^2(\varepsilon, i\omega_n) \left\{ \alpha^2 + \alpha \frac{|\Sigma_{AB}(i\omega_n)|^2}{[i\omega_n - \varepsilon - \Sigma_{AA}(i\omega_n)]^2} \right\} \\
&= \beta^{-1} \sum_{i\omega_n, \sigma} \int d\varepsilon\, V(\varepsilon) D(\varepsilon) \left[\alpha^2 G_{BB}^2(\varepsilon, i\omega_n) + \alpha |G_{AB}(\varepsilon, i\omega_n)|^2 \right],
\end{aligned}
\tag{A9}
$$

from which one can check that, if there is no orbital off-diagonal self-energy and $\alpha = \pm 1$, the kinetic energy is the same in the two orbitals. The computation of the current-current response in DMFT in infinite dimensions is simplified since all the vertex corrections are canceled [32] and only the elementary bubble contributions survive; therefore:

$$
\chi_{jj}(\mathbf{q}, \tau) = -\langle j_{\text{ex}}(\mathbf{q}, \tau) j_{\text{ex}}(-\mathbf{q}, 0) \rangle, \qquad j_{\text{ex}}(\mathbf{q}, \tau) = j_A(\mathbf{q}, \tau) - j_B(\mathbf{q}, \tau),
\tag{A10}
$$

$$
\chi_{jj}(\mathbf{q} \to 0, i\omega = 0) = \left[\chi_{jj}^{AA} - \chi_{jj}^{AB} - \chi_{jj}^{BA} + \chi_{jj}^{BB} \right](\mathbf{q} \to 0, i\omega = 0),
\tag{A11}
$$

$$
\chi_{jj}^{mm'}(\mathbf{q}, i\omega) = -\beta^{-1} \sum_{\mathbf{k}, iv, \sigma} v_{\mathbf{k}\sigma}^{(m)} v_{\mathbf{k}+\mathbf{q}\sigma}^{(m')} G_{mm'}(\mathbf{k}, iv) G_{m'm}(\mathbf{k} + \mathbf{q}, iv + i\omega), \qquad m, m' = A, B,
\tag{A12}
$$

where the current vertices for the two orbitals are related by $v^{(B)} = \alpha v^{(A)}$. Merging the DMFT results for the kinetic energy and the current-current response function, the superfluid stiffness for the selected model is

$$
\frac{D_S}{e^2 \pi} = -\frac{4\alpha}{\beta} \sum_{i\omega_n, \sigma} \int d\varepsilon\, V(\varepsilon) D(\varepsilon) |G_{AB}(\varepsilon, i\omega_n)|^2.
\tag{A13}
$$

This interesting result carries some important information. Since the superfluid stiffness must be a positive quantity, the naïve two-orbital Hubbard model with symmetric bands ($\alpha = 1$) would not allow any finite D_S. This is in agreement with some results showing that local excitonic correlations are dumped for $\alpha > 0$ [51] in favor of a bipartite antiferro-EC state that corresponds to a model with a shift of the B band of the vector $\mathbf{Q}$ of bipartite lattices for which $\epsilon_{\mathbf{k}} = -\epsilon_{\mathbf{k}+\mathbf{Q}}$, e.g., for the square lattice in D dimensions, the vector is $\mathbf{Q} = (\pi, \pi, ..., \pi)$. For $\alpha = 0$ (Falikov-Kimball model with spin), it correctly predicts no superfluid excitonic state since one of the species is not mobile and since, in this limit, no excitonic phase is expected [52]. This special case prohibits

excitonic ordering since, in the limit $\alpha \to 0^+$, there must be an antiferro-EC state, while in the limit $\alpha \to 0^-$, there must be a ferro-EC state; thus, $\alpha = 0$ is an unstable point between these two phases [29]. Our choice of opposite bands $\alpha = -1$ is therefore optimal, and in this situation, the superfluid stiffness can be rewritten as

$$
\frac{D_S}{e^2 \pi} = \frac{4}{\beta} \sum_{\sigma, i\omega_n} \int d\varepsilon\, V(\varepsilon) D(\varepsilon) |G_{AB}(\varepsilon, i\omega_n)|^2.
\tag{A14}
$$

This results tells us that the opposite band dispersion is the optimal ground for the research of a superfluid EC.

APPENDIX B: CALCULATION OF THE COHERENCE LENGTH

For the Bethe lattice, we have no access to the momenta but only energy; therefore, we must pass from $\nabla_{\mathbf{k}}$ to something we can treat. Starting from the numerator of the coherence length

definition [45,46]:

$$\sum_{\mathbf{k}} |\nabla_{\mathbf{k}} F(\mathbf{k})|^2 = \sum_{\mathbf{k}} \left| (\nabla_{\mathbf{k}} \epsilon_{\mathbf{k}}) \frac{\partial F(\epsilon)}{\partial \epsilon} \Big|_{\epsilon = \epsilon_{\mathbf{k}}} \right|^2 = \sum_{\mathbf{k}} \left| (\nabla_{\mathbf{k}} \epsilon_{\mathbf{k}}) \right.$$

$$\times \left[\frac{1}{\beta} \sum_{i\omega_n} \exp(i\omega_n 0^+) \frac{\partial}{\partial \epsilon} F(\epsilon, i\omega_n) \Big|_{\epsilon = \epsilon_{\mathbf{k}}} \right] \Big|^2,$$

(B1)

where $F(\epsilon, i\omega_n) = G_{AB}(\epsilon, i\omega_n)$, as previously defined (see Appendix A), and $\nabla_{\mathbf{k}} \epsilon_{\mathbf{k}} = v_{\mathbf{k}}$ is the group velocity of the non-interacting particles (we take $\hbar = 1$). Now the dependency on $\mathbf{k}$ is present only through $\epsilon_{\mathbf{k}}$ via the relation $|v_{\mathbf{k}}| = \sqrt{\frac{4t^2 - \epsilon_{\mathbf{k}}^2}{3}} = v(\epsilon)$; therefore, we can pass to the integral in energy, and the

result for the numerator is

$$\sum_{\mathbf{k}} |\nabla_{\mathbf{k}} F(\mathbf{k})|^2 = \int d\epsilon \, D(\epsilon) \left| \frac{1}{\beta} \sum_{i\omega_n} \exp(i\omega_n 0^+) v(\epsilon) \right.$$

$$\times \left. G_{AB}^2(\epsilon, i\omega_n) \frac{2\epsilon + \Sigma_{BB}(i\omega_n) - \Sigma_{AA}(i\omega_n)}{\Sigma_{AB}(i\omega_n)} \right|^2.$$

(B2)

For the denominator, no change is needed, and the substitution of $F(\mathbf{k})$ directly gives

$$\int d\epsilon \, D(\epsilon) \left| \frac{1}{\beta} \sum_{i\omega_n} \exp(i\omega_n 0^+) G_{AB}(\epsilon, i\omega_n) \right|^2. \qquad \text{(B3)}$$

[1] L. V. Keldysh and A. N. Kozlov, Sov. Phys. JETP **27**, 521 (1968).

[2] Y. Lozovik and V. Yudson, Sov. Phys. JETP **44**, 389 (1976).

[3] I. B. Spielman, J. P. Eisenstein, L. N. Pfeiffer, and K. W. West, Phys. Rev. Lett. **87**, 036803 (2001).

[4] J. P. Eisenstein and A. H. MacDonald, Nature (London) **432**, 691 (2004).

[5] G. W. Burg, N. Prasad, K. Kim, T. Taniguchi, K. Watanabe, A. H. MacDonald, L. F. Register, and E. Tutuc, Phys. Rev. Lett. **120**, 177702 (2018).

[6] J. Li, T. Taniguchi, K. Watanabe, J. Hone, and C. Dean, Nat. Phys. **13**, 751 (2017).

[7] A. Perali, D. Neilson, and A. R. Hamilton, Phys. Rev. Lett. **110**, 146803 (2013).

[8] I. Amelio, N. D. Drummond, E. Demler, R. Schmidt, and A. Imamoglu, Phys. Rev. B **107**, 155303 (2023).

[9] A. A. High, J. R. Leonard, M. Remeika, L. V. Butov, M. Hanson, and A. C. Gossard, Nano Lett. **12**, 2605 (2012).

[10] L. V. Butov, A. C. Gossard, and D. Chemla, Nature (London) **418**, 751 (2002).

[11] H. Cercellier, C. Monney, F. Clerc, C. Battaglia, L. Despont, M. G. Garnier, H. Beck, P. Aebi, L. Patthey, H. Berger *et al.*, Phys. Rev. Lett. **99**, 146403 (2007).

[12] A. Kogar, M. S. Rak, S. Vig, A. A. Husain, F. Flicker, Y. I. Joe, L. Venema, G. J. MacDougall, T. C. Chiang, E. Fradkin *et al.*, Science **358**, 1314 (2017).

[13] J. F. Afonso and J. Kuneš, Phys. Rev. B **95**, 115131 (2017).

[14] T. Moyoshi, K. Kamazawa, M. Matsuda, and M. Sato, Phys. Rev. B **98**, 205105 (2018).

[15] J. Kuneš and P. Augustinský, Phys. Rev. B **90**, 235112 (2014).

[16] G. Mazza, M. Rösner, L. Windgätter, S. Latini, H. Hübener, A. J. Millis, A. Rubio, and A. Georges, Phys. Rev. Lett. **124**, 197601 (2020).

[17] Y. Jia, P. Wang, C.-L. Chiu, Z. Song, G. Yu, B. Jäck, S. Lei, S. Klemenz, F. A. Cevallos, M. Onyszczak *et al.*, and Nat. Phys. **18**, 87 (2022).

[18] B. Sun, W. Zhao, T. Palomaki, Z. Fei, E. Runburg, P. Malinowski, X. Huang, J. Cenker, Y.-T. Cui, J.-H. Chu *et al.*, Nat. Phys. **18**, 94 (2022).

[19] S. De Palo, F. Rapisarda, and G. Senatore, Phys. Rev. Lett. **88**, 206401 (2002).

[20] P. López Ríos, A. Perali, R. J. Needs, and D. Neilson, Phys. Rev. Lett. **120**, 177701 (2018).

[21] S. De Palo, F. Tramonto, S. Moroni, and G. Senatore, Phys. Rev. B **107**, L041409 (2023).

[22] L. Rademaker, S. Johnston, J. Zaanen, and J. van den Brink, Phys. Rev. B **88**, 235115 (2013).

[23] X.-X. Huang, M. Claassen, E. W. Huang, B. Moritz, and T. P. Devereaux, Phys. Rev. Lett. **124**, 077601 (2020).

[24] X.-X. Huang, B. Moritz, M. Claassen, and T. P. Devereaux, Phys. Rev. B **105**, 165124 (2022).

[25] T. I. Vanhala, J. E. Baarsma, M. O. J. Heikkinen, M. Troyer, A. Harju, and P. Törmä, Phys. Rev. B **91**, 144510 (2015).

[26] T. Kaneko, K. Seki, and Y. Ohta, Phys. Rev. B **85**, 165135 (2012).

[27] J. Kuneš, Phys. Rev. B **89**, 115134 (2014).

[28] J. Kuneš, Phys. Rev. B **90**, 235140 (2014).

[29] J. Kuneš, J. Phys.: Condens. Matter **27**, 333201 (2015).

[30] A. Niyazi, D. Geffroy, and J. Kuneš, Phys. Rev. B **102**, 085159 (2020).

[31] A. Amaricci, G. Mazza, M. Capone, and M. Fabrizio, Phys. Rev. B **107**, 115117 (2023).

[32] A. Georges, G. Kotliar, W. Krauth, and M. Rozenberg, Rev. Mod. Phys. **68**, 13 (1996).

[33] M. Caffarel and W. Krauth, Phys. Rev. Lett. **72**, 1545 (1994).

[34] M. Capone, L. de' Medici, and A. Georges, Phys. Rev. B **76**, 245116 (2007).

[35] A. Amaricci, L. Crippa, A. Scazzola, F. Petocchi, G. Mazza, L. de Medici, and M. Capone, Comput. Phys. Commun. **273**, 108261 (2022).

[36] A. Koga, Y. Imai, and N. Kawakami, Phys. Rev. B **66**, 165107 (2002).

[37] For a spinless system, this is known as the exciton Mott phase [38].

[38] D. Guerci, M. Capone, and M. Fabrizio, Phys. Rev. Mater. **3**, 054605 (2019).

[39] A. Isidori, M. Berović, L. Fanfarillo, L. de' Medici, M. Fabrizio, and M. Capone, Phys. Rev. Lett. **122**, 186401 (2019).

[40] A. Richaud, M. Ferraretto, and M. Capone, Phys. Rev. B **103**, 205132 (2021).

[41] A. Scazzola, A. Amaricci, and M. Capone, Phys. Rev. B **107**, 085131 (2023).

[42] D. J. Scalapino, S. R. White, and S. C. Zhang, Phys. Rev. Lett. **68**, 2830 (1992).

[43] A. Toschi, M. Capone, and C. Castellani, Phys. Rev. B **72**, 235118 (2005).

[44] N. Verma, D. Guerci, and R. Queiroz, arXiv:2307.01253 [cond-mat.mes-hall] (2023).

[45] K. Seki, R. Eder, and Y. Ohta, Phys. Rev. B **84**, 245106 (2011).

[46] T. Kaneko and Y. Ohta, Phys. Rev. B **90**, 245144 (2014).

[47] G. Sangiovanni, A. Toschi, E. Koch, K. Held, M. Capone, C. Castellani, O. Gunnarsson, S.-K. Mo, J. W. Allen, H.-D. Kim *et al.*, Phys. Rev. B **73**, 205121 (2006).

[48] C. Taranto, G. Sangiovanni, K. Held, M. Capone, A. Georges, and A. Toschi, Phys. Rev. B **85**, 085124 (2012).

[49] G. Sangiovanni, M. Capone, C. Castellani, and M. Grilli, Phys. Rev. Lett. **94**, 026401 (2005).

[50] G. Sangiovanni, M. Capone, and C. Castellani, Phys. Rev. B **73**, 165123 (2006).

[51] P. Farkasovsky, Cond. Mat. Phys. **23**, 43709 (2020).

[52] P. Farkasovsky, Phys. Rev. B **65**, 081102(R) (2002).